Energy Conversion and Management 174 (2018) 504–515

Contents lists available at ScienceDirect

Energy Conversion and Management

journal homepage: www.elsevier.com/locate/enconman

Effect factors of part-load performance for various Organic Rankine cycles using in engine waste heat recovery

Xuan Wang[a,b], Gequn Shu[a,*], Hua Tian[a,*], Wei Feng[b], Peng Liu[a], Xiaoya Li[a]

[a] State Key Laboratory of Engines, Tianjin University, No. 92, Weijin Road, Nankai District, Tianjin 300072, China
[b] Energy Technologies Area, Lawrence Berkeley National Laboratory, 1 Cyclotron Road, Berkeley, CA 94720, USA

ARTICLE INFO

Keywords:
Dynamic process
Waste heat recovery
Organic Rankine Cycle
Part-load
Engine

ABSTRACT

The Organic Rankine Cycle (ORC) is regarded as one of the most promising waste heat recovery technologies for electricity generation engines. Since the engine usually operates under different working conditions, it is important to research the part-load performance of the ORC. In order to reveal the effect factors of part-load performance, four different forms of ORCs are compared in the study with dynamic math models established in SIMULINK. They are the ORC applying low temperature working fluid R245fa with a medium heat transfer cycle, the ORCs with high temperature working fluid toluene heated directly by exhaust condensing at low pressure and high pressure, and the double-stage ORC. It is regarded that the more slowly the system output power decreases, the better part-load performance it has. Based on a comparison among the four systems, the effects of evaporating pressure, condensing condition, working fluid, and system structure on part-load performance are revealed in the work. Further, it is found that the system which best matches with the heat source not only performs well under the design conditions, but also has excellent part-load performance.

1. Introduction

The ORC (Organic Rankine Cycle) is one of the most promising energy conversion technologies for electricity generation engine waste heat recovery [1]. The former study shows that the engine power can be increased by about 10–17% with the ORC [2–5]. Additionally, the ORC shows great flexibility, high safety, low cost, and low maintenance requirements [6]. In recent years, a number of engine-ORC combined systems have been installed, for example in Italy at Pavia (0.6 MW), Portogruaro (0.6 MW), Catania (0.6 MW), Pescara (0.7 MW), Chivasso (1 MW), Pisticci (1.8 MW) and Pisticci Scalo (4 MW); in Germany at Kempen (0.6 MW) and Senden (1 MW); and in Finland at Ammassuo, Espoo (1.3 MW) [2,7].

There are a number of different kinds of ORCs for engine waste heat recovery. In our previous research [8], the most common basic ORCs are classified as: the ORC with low temperature working fluid such as refrigerants, named LT-ORC; the ORC with high temperature working fluid such as benzenes, named HT-ORC; and the double-stage ORC, named DORC or binary ORC [9]. Comprehensive evaluation of different ORCs has been studied based on the first and second laws of thermodynamics, and the economy, revealing their own advantages and disadvantages, respectively. For example, Vaja and Gambarotta [10] compared the performance of LT-ORCs (R245fa and R11 working fluids) and the HT-ORC (benzene working fluid) as the WHRS (waste heat recovery system) for an internal combustion engine. It was found that the largest efficiency increase of the engine could be obtained by the ORC with benzene, while the smaller and cheaper turbine could be applied in the LT-ORC. Shu et al. [11] compared the performance of a single-loop ORC and a DORC as the WHRS of a heavy-duty diesel engine, based on a multi-approach evaluation system. It was demonstrated that the DORC system was a suitable configuration for engine waste heat recovery, as it performed excellently during thermodynamic and economic evaluating processes. The research of Invernizzi and Nadeem [9] showed performance limitations in simple cycles under realistic assumptions, such as the application of a single-stage turbine, and revealed the high efficiency of binary ORC (15–16%).

All of the above research focuses solely on steady performance under design working conditions. In fact, working conditions for electricity generation engines often vary, leading to large and frequent changes in waste heat [12,13], so it is crucial to study the part-load performance of ORCs [12]. Part-load performance can be predicted by the static off-design model and the dynamic model [10]. The static off-design model can calculate part-load performance under different stable working conditions, but it cannot reflect dynamic behavior in an unsteady state. On the other hand, it does not require much calculation resource. The whole dynamic varying process of the ORC can be figured

* Corresponding authors.
E-mail addresses: sgq@tju.edu.cn (G. Shu), thtju@tju.edu.cn (H. Tian).

https://doi.org/10.1016/j.enconman.2018.08.024
Received 27 April 2018; Received in revised form 6 August 2018; Accepted 7 August 2018

Nomenclature

T	temperature (K)
ρ	density (kg/m^3)
α	heat transfer coefficient (W/m^2 K)
C_p	specific heat (J/kg K)
m	mass flow rate (kg/s)
A	area (m^2)
t	time (s)
D	diameter (m)
h	specific enthalpy (J/kg)
Re	Reynolds number
Nu	Nusselt number
Pr	Prandtl number
γ	void fraction (m^2/s)
μ	density ratio
u	velocity (m/s)
L	length (m)
p	pressure (Pa)
x	vapor quality
ω	revolution speed (rpm)
η_v	volumetric efficiency
V_{cyl}	cylinder volume (m^3)
$\dot{V}$	volume flow rate (m^3/s)
C_v	turbine coefficient
W	work (kW)
Q	absorbed heat (kW)
η_{st}	isentropic efficiency of expander
η	dynamic viscosity (Pa s) or liquid fraction or efficiency
η_{sp}	isentropic efficiency of pump
c_s	isentropic gas speed(m/s)

Subscript

l	liquid
g	gas
e	heat source
c	cold
f	fluid
i	inside
o	outside
w	wall
in	inlet
out	outlet
r	working fluid
avg	average
p	pump
s	isentropic
t	turbine
rec	receive
amb	ambient

Abbreviation

ORC	Organic Rankine Cycle
DORC	Dual-loop Organic Rankine Cycle
B-ORC	back pressure ORC
C-ORC	condensing ORC
MB	moving Boundary
WHRS	Waste Heat Recovery System
HT	high temperature
LT	low temperature

out by the dynamic model, which can be used to develop the control system, but doing so requires more calculation resource than the static model.

Fu et al. [14] investigated the effects of heat source temperature on ORC system part-load performance by the static part-load model. It was found that the heat source temperature variation of −10.3 °C to +19.8 °C from the design value resulted in variations of −13.6% to +22.6% and −11.5% to +17.4% in net output power and thermal efficiency, respectively. Badescu et al. [15] conducted a study on recovering exhaust waste heat from a power generation engine under different engine working conditions using the static part-load model. When the engine was coupled with an ORC, the overall thermal efficiency of the combined system could be higher than that of the engine alone by 6.00%, 5.85%, and 5.91% under engine loads of 100%, 75%, and 50%, respectively. Bamgbopa and Uzgoren [16] established both static and dynamic models of the ORC. The static model was used to develop a static state map to construct a control strategy. The dynamic model was used to study system part-load performance when the heat source gradually or abruptly varied with and without the control strategy. It was demonstrated that adjusting flow rates could not only improve thermal efficiency but also help to maintain steady state operation. Danov and Gupta [17] proposed a combined cycle which used the diesel engine as the top cycle and the ORC as the bottom cycle for exhaust waste heat recovery. A numerical dynamical model was established to assess part-load performance under different engine working conditions, and this showed tight interactions between the two cycles when the engine was not running under full load. Horst et al. [18] established a dynamic ORC model with a controller as the WHRS of an automotive engine to evaluate fuel saving potential during an exemplary dynamic motorway driving scenario. The results showed that the WHRS could improve fuel economy by 3.4%. Mazzi et al. [19] presented a dynamic model of an LT-ORC for exhaust waste heat recovery. Results showed that system efficiency at the design point only slightly decreased (from 24.45% to 24.21%) in the range of 80–110% of the nominal oil mass flow rate at constant temperature. By contrast, changes in oil temperature affected efficiency significantly.

All of the above researches about ORC part-load performance focus solely on the performance variation of a certain system when the parameters of the heat source or the ORC itself change. There are few studies that focus on comparing the part-load performance of different ORCs and finding the effect factors. Therefore, the part-load performance of different ORCs as the WHRS of an electricity generation engine is compared under different working conditions by the dynamic model with a control system in this study. As mentioned above, the most common basic ORCs are classified as LT-ORC, HT-ORC, and DORC, with HT-ORCs being divided into systems with high condensing pressure and low condensing pressure. Consequently, four different ORC configurations in total are compared. Based on this, the reasons why they perform differently under part-load conditions are analyzed in detail.

2. System description

2.1. The engine

The electricity generation engine in this study is a natural gas internal combustion engine of 1000 kW rated power. The heat balance experiments on the engine have been conducted by our research group, which aimed to understand the distribution of output energy under full engine working conditions, such as the proportion of effective power, exhaust heat, jacket water heat, and so on. However, in this work only the exhaust, which is the most important waste heat source and accounts for about 30–40% of input energy, is the heat source for different ORCs. Therefore, only the parameters related to exhaust under seven

typical working conditions are shown in Table 1. As the power plant, it keeps a constant speed (600 rpm) while its load varies according to demand. Therein, the exhaust mass flow rate is hard to measure directly because of its high temperature and corrosivity, so it is calculated with the measurement of intake air volume flow rate and the heat consumption rate of natural gas.

2.2. Investigated ORC configurations

In the study, the most common ORCs are classified as LT-ORC, HT-ORC, and DORC, with HT-ORCs being divided into systems with high condensing pressure (B-ORC) and low condensing pressure (C-ORC). In total, four different ORCs are compared.

There are a number of different organic working fluids, and much research focuses on the selection of working fluids, such as Refs. [20–22]. Based on their respective heat source temperature and critical temperature ranges, working fluids can be classed as low temperature (LT) working fluids or high temperature (HT) working fluids [23,24]. The critical temperature, normal boiling temperature, and decomposition temperature of LT working fluids are all usually relatively low. If they are heated directly by high temperature exhaust, they may resolve. In that case, a medium heat transfer cycle would be required [25–27]. Fig. 1 shows the structure of an LT-ORC that applies pressured hot water as the medium heat transfer cycle. R245fa is selected to represent LT-ORCs in the study. Another feature of LT-ORCs is that they often condense under environment temperature with positive condensing pressure, because of their low normal boiling temperature.

HT working fluids such as alkanes and siloxanes usually have a high critical temperature, a normal boiling temperature, and a relatively high decomposition temperature. They have been applied widely in high temperature waste heat recovery [28–30]. Some of them, such as toluene, remain remarkably stable at high temperature [31], so they can be heated by exhaust directly [28–30] as shown in Fig. 2. Toluene is selected to represent HT-ORCs in the study. HT-ORCs can produce large output power, condensing under the environment temperature. However, owing to HT-ORCs' high normal boiling temperature, their condensing pressure is quite low and their pressure ratio in turbines is very great, making turbine manufacture difficult [9,30]. Therefore, in many applications the condensing pressure and temperature of HT-ORCs are increased to offer heating [32,33] or cooling [34,35] as the cogeneration system. HT-ORCs with low condensing pressure and high condensing pressure are named C-ORC and B-ORC, respectively, in the study.

The DORC is a 'binary cycle' of the B-ORC and LT-ORC as described in Fig. 3. The first cycle is directly heated by the exhaust and condensates under high temperature. Therefore, the condensing heat can be sequentially recovered by another LT-ORC. A high temperature cooling water cycle connects the two ORCs, which makes the whole system safe and flexible for offering cooling, heating, or electricity [36]. The DORC can avoid the vacuum degree in the condenser and a too large pressure ratio in the HT-ORC, while still outputting a large amount of power roughly equivalent to that of a C-ORC [9,30]. The working fluids of the first and second cycles are toluene and R245fa for the DORC in the study. Fig. 4 shows the T-s diagram of the four kinds of ORCs. Toluene and R245fa are both dry fluids, so just a small superheat degree is required to protect the turbine [37].

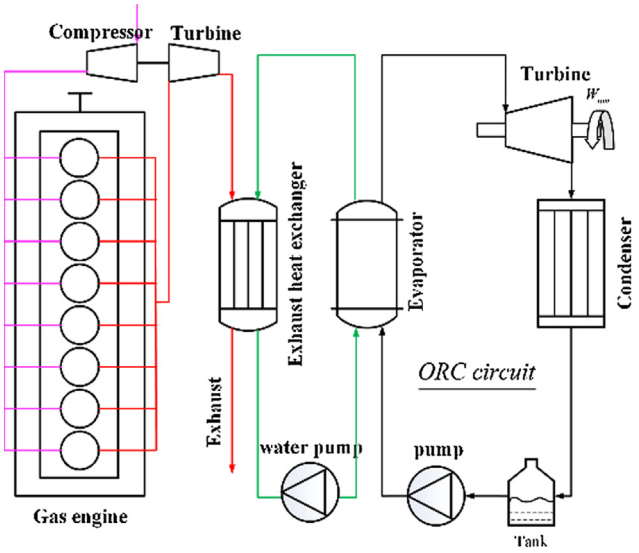

Fig. 1. The system structure of LT-ORC.

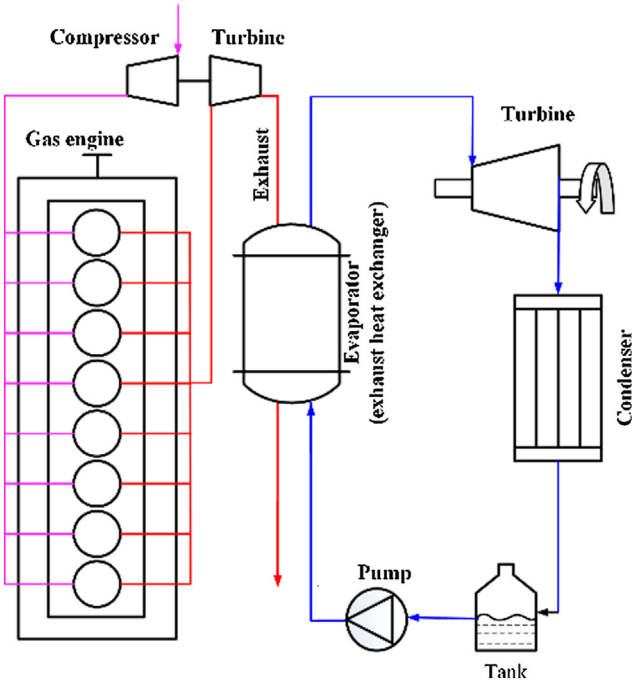

Fig. 2. The system structure of B-ORC and C-ORC.

Table 1
Main parameters of the engine.

Parameter	Unit	Value						
Speed	r/min	600	600	600	600	600	600	600
Work condition load	/	40%	50%	60%	70%	80%	90%	100%
Effective power	kW	400	500	600	700	800	900	1000
Exhaust temperature	°C	470	515	525	527	530	532	540
Heat consumption rate of gas	MJ/kWh	13.09	11.76	11.08	10.59	10.20	10.26	9.85
Intake air volume flow rate	m^3/h	1774	2145	2465	2748	3120	3510	4180
Exhaust mass flow rate	kg/s	0.711	0.859	0.987	1.101	1.258	1.414	1.563

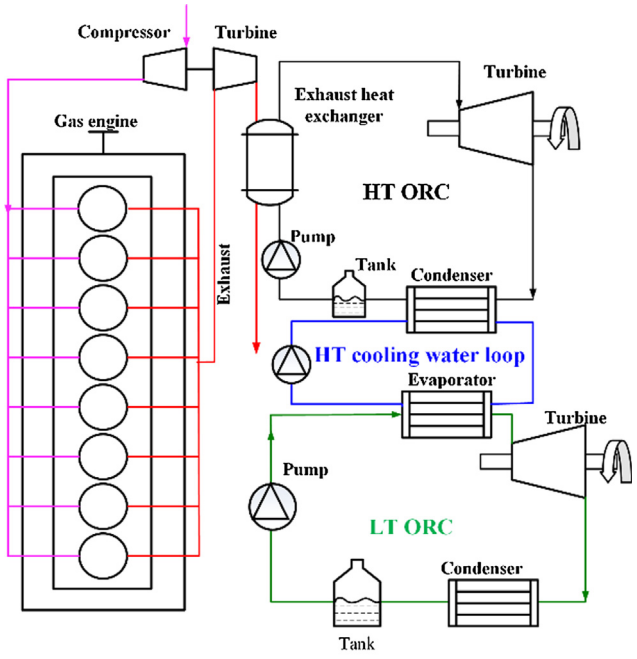

Fig. 3. The system structure of DORC.

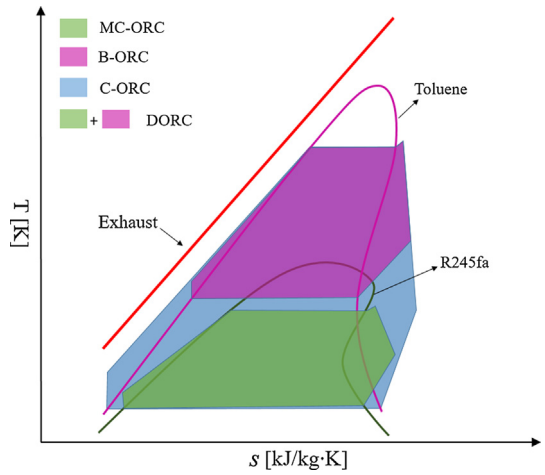

Fig. 4. The T-s diagram of the four systems.

3. Dynamic model

The dynamic models are established here to research the part-load performance of the four different ORCs. Firstly, the dynamic models of the main components in every system are established and then are combined together to create the whole system model based on their interrelationships. Since pumps and expanders respond much faster than heat exchangers, their models are usually replaced by static models [38,39]. The math model is built by SIMULINK and the property parameters of working fluids are obtained from REFPROP.

3.1. The heat exchangers with phase change

Because there is phase change in the evaporator and the convective heat transfer coefficients of various phases are quite different, the dynamic model is established by the MB (moving boundary) method. The MB method has been regarded as the most popular and effective approach for dynamic modeling of heat exchangers with phase change, and has proven to be precise enough with experimental data [39]. With the MB method, the working fluid side of the evaporator is divided into three regions: the sub-cooling region, the two-phase region, and the super-heating region as shown in Fig. 5. The lumped parameter method is applied in every region.

The general differential mass balance equation of the three regions is:

$$\int_0^{Li} \frac{\partial(A\rho)}{\partial t} dz + \int_0^{Li} \frac{\partial \dot{m}}{\partial z} dz = 0 \tag{1}$$

The general differential energy balance equation of the three regions is:

$$\int_0^{Li} \frac{\partial(A\rho h - Ap)}{\partial t} dz + \int_0^{Li} \frac{\partial \dot{m} h}{\partial z} dz = \int_0^{Li} \alpha_i \pi D_i (T_w - T_r) dz \tag{2}$$

A simplified energy balance equation of the wall is:

$$c_{pw}\rho_w A_w \frac{dT_w}{dt} = \alpha_i \pi D_i (T_r - T_w) + \alpha_o \pi D_o (T_a - T_w) \tag{3}$$

Integrating the three Eqs. (1)–(3) over every region respectively, MB models for the evaporator can be obtained. More detail about the MB method can be found in [38].

Corresponding to the three regions of working fluid, the heat source side can also be divided into three regions. The heat source for the evaporator in different ORCs in the study can be exhaust or hot water, as shown in Figs. 1–3. The dynamic response of hot water cannot be ignored, so a dynamic model is adopted. Because the heat capacity and density of exhaust is small, it responds much faster than working fluid or hot water. Therefore, a static model can be used [40,41]. Static and

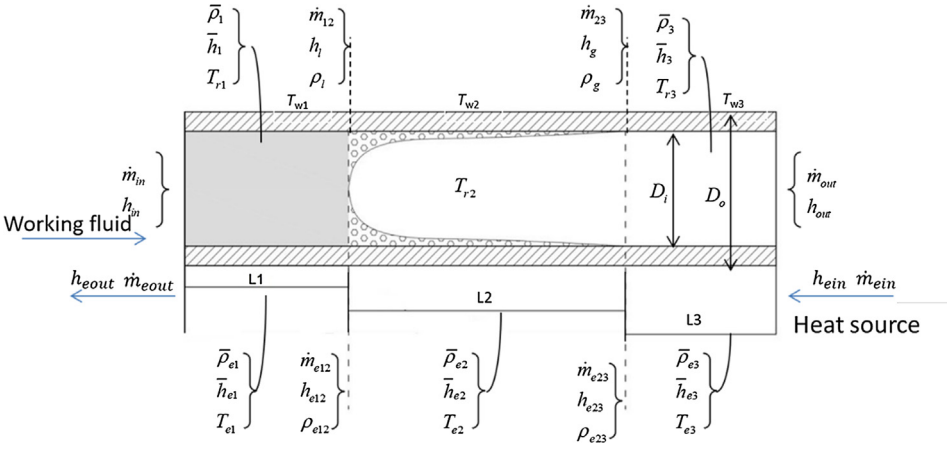

Fig. 5. The schematic of the MB model with three regions.

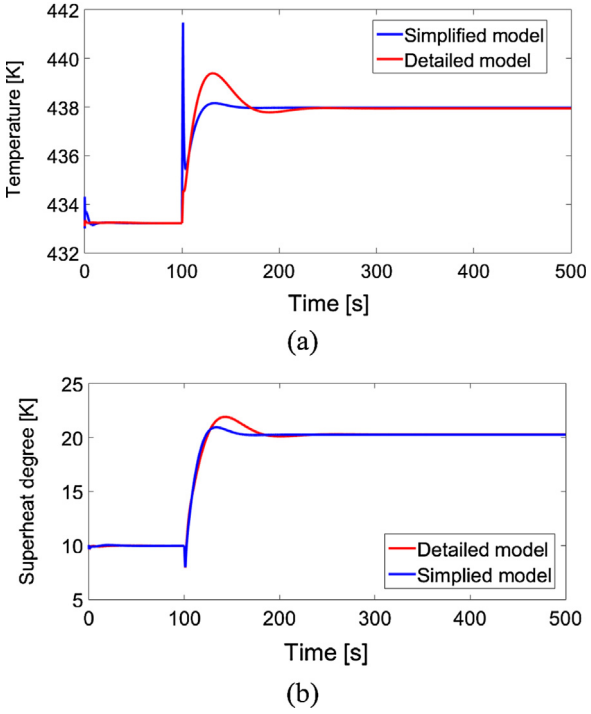

Fig. 6. The comparison between the static and dynamic models of the exhaust. (a) The variation of the final exhaust temperature. (b) The variation of the fluid superheat degree.

dynamic models of the exhaust are compared to show their suitable application range in Fig. 6. For the dynamic model, the general energy and mass balance Eqs. (1) and (2) are suitable for exhaust or hot water as well. In Refs. [40,41], the exhaust static model only contains the energy balance as shown in Eq. (4). Therein, subscript i represents different phase regions.

$$m_e(h_{i\_ein}-h_{i\_eout}) = \alpha_i \pi D_i L_i (T_{ei}-T_{wi}) \tag{4}$$

The dynamic variation processes for the static model and dynamic model of the exhaust are compared in Fig. 6. This figure describes the changing of the outlet exhaust temperature (at the evaporator outlet) and the superheat degree at turbine inlet when the mass flow rate of working fluid toluene decreases. It can be seen that the stable values of the two models are the same, while the dynamic processes are very different. Obviously, the exhaust temperature and superheat degree of the static model respond faster than in the dynamic model. Further, the variation of exhaust temperature in the static model is not smooth, because it ignores the dynamic of exhaust. However, if only the static part-load performance is needed, the static model is a good choice due to its simplicity of calculation.

A dynamic model of the condenser is also established by the MB method, and it is quite similar to that of the evaporator. There should be a drum after the condenser as shown in Figs. 1–3. This is not only for the safety of the pump, but also for the stability of the whole dynamic system model. The model of the drum can be expressed as:

$$\frac{dm_{rec}}{dt} = \dot{m}_{rec,in}-\dot{m}_{rec,out} \tag{5}$$

$$\frac{d(m_{rec}u_{rec})}{dt} = \dot{m}_{rec,in}h_{in}-\dot{m}_{rec,out}h_{out} + UA(T_{amb}-T_{rec}) \tag{6}$$

3.2. The heat exchangers without phase change

There is no phase change in the exhaust exchanger of the LT-ORC and the exhaust temperature drops greatly, so the discrete method is used for this heat exchanger as shown in Fig. 7. The model can be described as:

Hot water:

$$A_1\Delta x\bar{\rho}_{f1,ai}\overline{C}p_{f1,ai}\frac{d\overline{T}_{f1,ai}}{dt} = \alpha_{in,i}\pi D_i\Delta x(T_{w,i}-T_{f1,ai}) + \dot{m}_{f1}h_{f1,i}-\dot{m}_{f1}h_{f1,i+1} \tag{7}$$

Exhaust:

$$A_2\Delta x\left(\bar{\rho}_{f2,ai}\frac{\partial\overline{h}_{f2,ai}}{\partial\overline{T}_{f2,ai}} + \bar{h}_{f2,ai}\frac{\partial\bar{\rho}_{f2,ai}}{\partial\overline{T}_{f2,ai}}\right)\frac{d\overline{T}_{f2,ai}}{dt} = \alpha_{out,i}\pi D_o\Delta x(T_{w,i}-T_{f2,ai}) + \dot{m}_{f2}h_{f2,i+1}-\dot{m}_{f2}h_{f2,i} \tag{8}$$

Pipe wall:

$$A_w\Delta x\rho_w Cp_w\frac{d\overline{T}_{w,ai}}{dt} = \alpha_{out,i}\pi D_o\Delta x(T_{f2,ai}-T_{w,i}) + \alpha_{in,i}\pi D_i\Delta x(T_{f1,ai}-T_{w,i}) \tag{9}$$

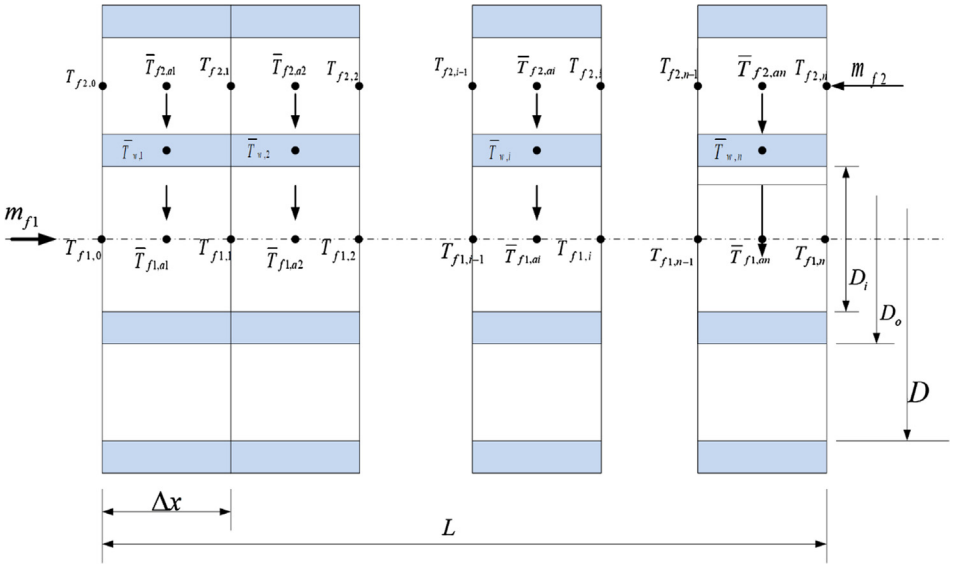

Fig. 7. The discretization model of the water heat exchanger.

Table 2
The heat transfer coefficients used in the model.

Heat transfer side	Heat transfer coefficients	
Exhaust side [42]	$\frac{D_i\alpha_f}{\lambda} = 0.1378\left(\frac{D_i G_{max}}{\mu}\right)^{0.718}\left(\frac{c_p\mu}{\lambda}\right)^{1/3}\left(\frac{S_f}{H_f}\right)^{0.296}$	(10)
Hot water side/cooling water side [43]	$Nu_f = C_\alpha Re^m Pr_f^{0.36}(Pr_f/Pr_w)^{0.25}$	(11)
Inside tube (single phase) [43]	$Nu_f = 0.027 Re_f^{0.8} Pr_f^{1/3}\left(\frac{\eta_f}{\eta_w}\right)^{0.14}$	(12)
Inside tube (two-phase) [44]	$\alpha = \alpha_l\left\{\left[(1-x) + 1.2x^{0.4}(1-x)\left(\frac{\rho_l}{\rho_g}\right)^{0.37}\right]^{-2.2} + \left[\frac{\alpha_g}{\alpha_l}x^{0.01}(1+8(1-x)^{0.7})\left(\frac{\rho_l}{\rho_g}\right)^{0.67}\right]^{-2}\right\}^{-0.5}$	(13)

3.3. Heat transfer coefficient

All heat transfer coefficients used in the model are shown in Table 2. In order to enhance heat transfer with exhaust, there are fins in all of the exhaust heat exchangers but not in the hot water exchanger. More detail about the heat transfer coefficients can be found in the corresponding literature [42–44].

3.4. Pump and turbine

A displacement pump is applied in the study and the mass flow rate can be expressed as [38]:

$$m_{pump} = \eta_v \cdot \rho_{pump} \cdot V_{cyl} \cdot \omega \tag{14}$$

Therein, η_v, ρ_{pump}, V_{cyl}, and ω are the volumetric efficiency, the density of the working fluid at the pump inlet, the cylinder volume, and pump speed. The working fluid experiences a non-isentropic process in the pump. The ideal working fluid enthalpy after isentropic pumping is h_{spout}. h_{pin} and h_{pout} are the enthalpy of working fluid at the inlet and outlet of the pump, respectively. η_{sp} is the isentropic pump efficiency and η_g is the efficiency of the electromotor, which are assumed to be 0.7 and 0.9, respectively. Then the consumed work of the pump is:

$$W_p = m(h_{pout} - h_{pin})/\eta_g \tag{15}$$

$$h_{pout} = h_{pin} + (h_{spout} - h_{pin})\cdot\eta_{sp} \tag{16}$$

The turbine can be simplified as a nozzle [38]. Since the pressure ratio (the ratio of the pressure before and after the turbine) is much greater than the critical pressure ratio of the working fluid, the fluid reaches supersonic speed under most conditions, and the influence of turbine outlet pressure can therefore be ignored [45]:

$$\dot{m}_t = C_v\sqrt{\rho_{in} p} \tag{17}$$

Therein, C_v is a coefficient, ρ_{in} is the working fluid density at the inlet of the turbine, and p is the evaporating pressure. In the turbine, the working fluid experiences a non-isentropic process and the calculation of turbine power is similar to the pump:

$$W_t = m(h_{tin} - h_{tout})\eta_g \tag{18}$$

$$h_{tout} = h_{tin} - (h_{tin} - h_{sout})\eta_{st} \tag{19}$$

The turbine efficiency η_{st} designed as 0.7 varies under different part-load conditions, and is expressed as an empirical equation with several empirical coefficients in most part-load performance research [46,47]. These empirical coefficients are very important and change with different working fluids, different manufactures, and so on. Since the output power of the four ORCs is compared in the paper, the selection of empirical coefficients greatly affects results. However, it is not reasonable to make these empirical coefficients identical for all the four ORCs, because they have different working fluids. In order to avoid the effects of different turbines, the isentropic turbine efficiency is assumed as constant. When doing the research on part-load performance of only one specific ORC system, it is suggested to use a generic dimensionless curve of the turbine efficiency.

Fig. 8. The experiment bench for ORC dynamic model validation.

3.5. Model validation

In order to validate the dynamic ORC model, the experiment bench has been established as shown in Fig. 8. The experiment system is a basic ORC with working fluid R245fa, which mainly consists of evaporator, turbine (replaced by expansion valve in this system), condenser, tank, pump, and some sensors. Fig. 9 gives a clear structure description of the system. The experiment bench aims at validating the dynamic ORC model and developing control systems in the future, so it is a principle experiment system with small capacity. The design absorption heat of the evaporator is 10 kW and it is heated by the hot air generated from an electrical heater.

The model is validated by comparing the dynamic process of several important parameters with experiment measurement when decreasing the working fluid mass flow rate. Therefore, the experiment process can be simply described as:

1. Make the system work in a stable condition for a while and record the data.
2. Change the working fluid mass flow rate by adjusting the pump and record the whole dynamic variation process.
3. Repeat this experiment several times and select the best group of data.

The dynamic model is designed according to the real parameters of the experiment system and its stable state in the above process. It is hard to calculate the exact heat transfer coefficients, so they need to be modified based on the experiment measurement [48]. After finishing the design, the stable state of the model mostly agrees with the experiment measure as shown in Figs. 10–12. Figs. 10–12 compare the dynamic variation of the model and experiment when the working fluid

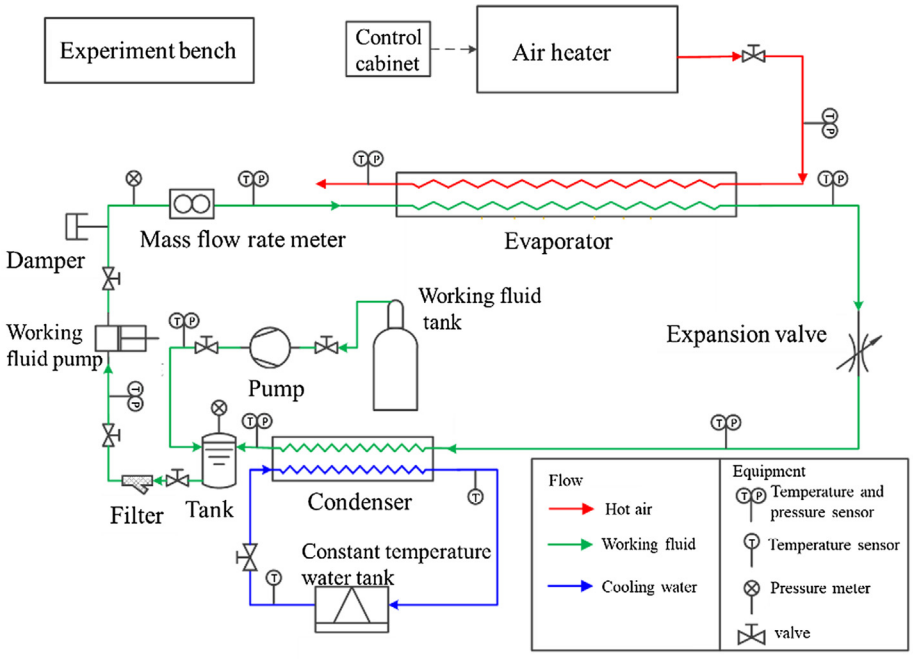

Fig. 9. The detailed structure of the experiment bench.

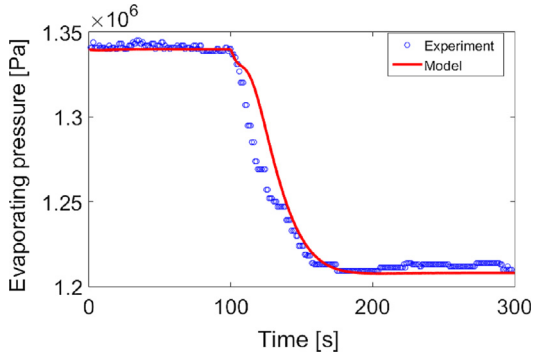

Fig. 10. The validation of evaporating pressure.

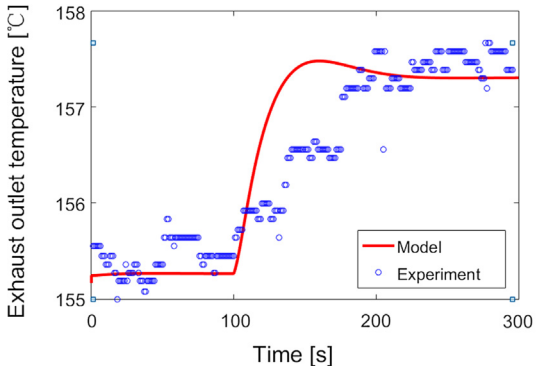

Fig. 12. The validation of hot air temperature at the evaporator outlet.

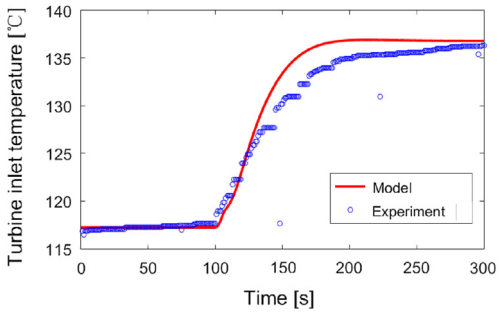

Fig. 11. The validation of working fluid temperature at the turbine inlet.

mass flow rates decrease by the same value. It can be seen that the model has enough consistency with the experiment.

4. Results and discussion

In this part, firstly the part-load performance of three kinds of single-stage ORCs under seven typical engine working conditions is compared. The three engines are the LT-ORC with working fluid R245fa, the B-ORC, and the C-ORC with working fluid toluene. All are designed based on the rated engine working condition and main design parameters are shown in Table 3. It should be noted that since the heat exchange tubes in the exhaust heat exchangers of all three ORCs have the same structure parameters, as well as the condensers, the length of tube is used to represent heat transfer area. The exhaust temperature out of the exhaust heat exchanger (i.e., final exhaust temperature) should be higher than the acid dew point, otherwise the equipment can be corroded [49]. The acid dew point varies with sulphur content and is assumed as 383 K in the paper. According to our former research [50], the final exhaust temperature declines as the engine working condition decreases. Therefore, if another control strategy is not adopted, the design final exhaust temperature should be high enough above the acid

Table 3
The main design parameters of the three single-stage ORCs.

System	LT-ORC	B-ORC	C-ORC
Exhaust heat exchanger tube length (m)	82.68	236.19	163.68
Condenser tube length (m)	239.0	45.72	112.89
Working fluid mass flow rate (kg/s)	2.7225	1.2918	0.9497
Condensing temperature (K)	308.15	409.56	308.15
Condensing pressure (kPa)	211	200	6.24
Evaporating pressure (MPa)	2.0	2.0	2.0
Cooling water temperature (K)	298.15	358	298.15
Cooling water mass flow rate (kg/s)	30	30	30

dew point to avoid corrosion under part-load conditions. As a result, the design final exhaust temperature is 50 K higher than the acid point in this work. The condensing temperature of the B-ORC is much higher than the environment temperature and in order to utilize the condensing heat, the design cooling water temperature is high. Then the DORC is compared with the three single-stage ORCs in Section 4.2.

4.1. The part-load performance comparison of the three single stage systems

Fig. 13 describes the dynamic variation of the output power of the three ORCs when the engine working condition decreases by 10% every 700 s. In other Figs. (i.e., Figs. 15, 18, and 19), the engine working condition decreases like this as well. It can be seen that under the rated engine working condition, the power of the B-ORC is slightly less than that of the LT-ORC, while with the dropping working condition B-ORC begins to exceed LT-ORC. Therefore, the B-ORC output power declines more slowly than the LT-ORC and has better part-load performance. The power of the C-ORC is much larger than the other two, so in order to compare them intuitively the dimensionless power is shown in Fig. 14. Dimensionless power is defined as the output power under the part-load condition divided by that under the rated condition. The larger the dimensionless power is, the more slowly the power decreases and the better part-load performance the system has. From the figure, it can be found that the power of the C-ORC declines most slowly and the B-ORC comes second. The LT-ORC has the worst part-load performance. Further, the difference among them becomes greater and greater as the working condition declines. The output power is equal to the product of absorbed heat and thermal efficiency, so the part-load performance differences will be analyzed from these two aspects, especially efficiency.

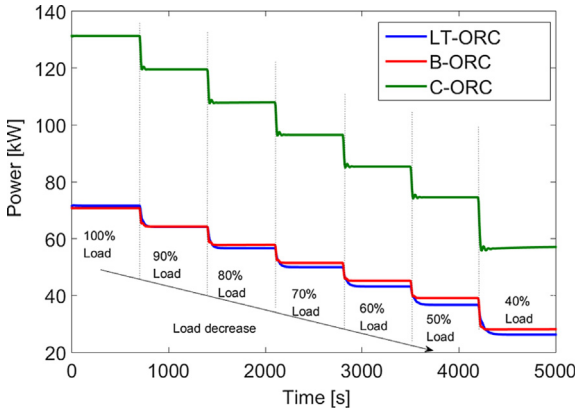

Fig. 13. The output power of the three single-stage ORCs under seven typical engine working conditions.

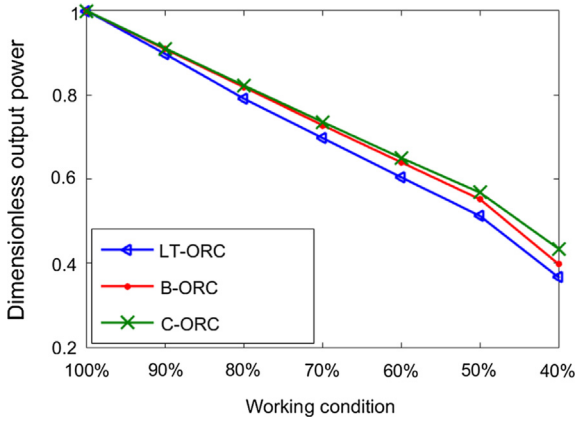

Fig. 14. The dimensionless output power of the three single-stage ORCs under seven typical engine working conditions.

4.1.1. The analysis of the absorbed heat

Fig. 15 describes the variation of the final exhaust temperature when the engine condition changes, and the stable values of absorbed heat under the seven conditions are shown in Fig. 16. The dynamic model of the exhaust is applied in the LT-ORC model, so the dynamic behavior of the final temperature is smooth. By contrast, the static model is applied in the other two systems, leading to a rough process. Nevertheless, the stable values are the same as analyzed in Part 3. The final exhaust temperature of the B-ORC is always highest, so it absorbs the least heat. The final exhaust temperature of the LT-ORC is slightly higher than that of the C-ORC, except under the 40% working condition. Additionally, as the working condition declines, the final exhaust temperature of the B-ORC becomes increasingly higher than the others. Under the 40% working condition, the final exhaust temperature of the B-ORC is 40 K higher than that of the LT-ORC, which means the absorbed heat is almost 20 kW less.

It is well known that the absorbed heat is decided by the product of the total heat transfer coefficient, the area, and the temperature difference. Therein, the heat transfer area is fixed, so the difference of absorbed heat under part-load is decided by the product of the other two factors. The exhaust heat exchangers in the three systems have the same structure and geometrical parameters except for heat transfer area. Therefore, all heat transfer coefficients on the exhaust side are nearly the same. In the B-ORC and C-ORC, the heat transfer coefficients on the working fluid side are much larger than those on the exhaust side. Since the overall heat transfer coefficients are greatly affected by the smaller one, both systems have approximate overall heat transfer coefficients and changing of the temperature difference plays a decisive role. Under the design condition, all systems have the same absorbed heat, while the heat transfer area of the exhaust heat exchanger in B-ORC is much larger than that in the C-ORC. This indicates the average temperature difference of the B-ORC is much smaller, so the reduction

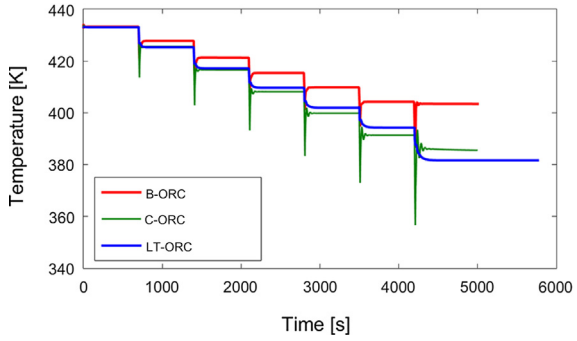

Fig. 15. The variation of final exhaust temperatures of the three single-stage ORCs under seven typical engine working conditions.

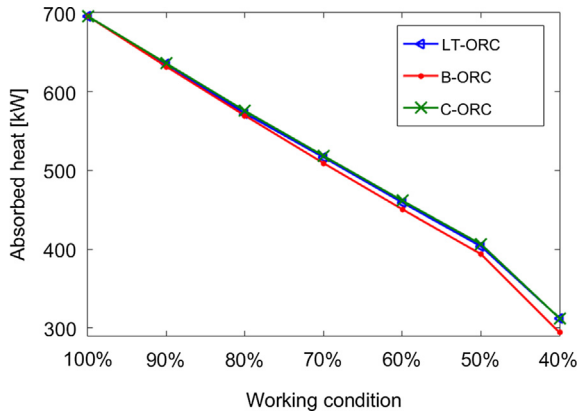

Fig. 16. The absorbed heat of the three single-stage ORCs under seven typical engine working conditions.

of heat transfer ability is more sensitive to the decrease in temperature difference. In other words, when the engine working condition decreases, leading to a drop in heat transfer temperature difference, the B-ORC with the larger heat transfer area and smaller temperature difference will be affected more obviously and absorb less heat as described in Figs. 15 and 16. It is difficult to compare the LT-ORC with the former two systems by a certain main factor because it exchanges heat twice and the heat transfer model is complex. According to the calculation results, its absorbed heat is similar to that of the C-ORC under the seven engine working conditions.

4.1.2. The analysis of thermal efficiency

The absorbed heat of the B-ORC reduces fastest with declining engine working condition, while its output power decreases more slowly than the LT-ORC, which means that the thermal efficiency of the B-ORC must also decrease more slowly than the LT-ORC. Similarly, the efficiency of the LT-ORC must decrease fastest because it absorbs approximately the same heat as the C-ORC under different working conditions, while its power is the least. The stable values of the thermal efficiencies of the three systems are shown in Fig. 17. Just as in the analysis above, the LT-ORC efficiency decreases the most quickly. The ORC thermal efficiency is mainly decided by the evaporating pressure, the condensing pressure, and the superheat degree. Therein, the superheat degree is controlled as 10 K. Consequently, the differences of the efficiencies under part-load will be analyzed in detail from the evaporating pressure and condensing pressure in the below.

Figs. 18 and 19 describe the variation of the evaporating pressures and the condensing pressures in the three systems when the engine working condition changes. It can be found that the difference among the evaporating pressures of the three systems is not very large. By contrast, there is obvious distinction among the condensing pressures. As the engine working condition decreases, both the absorbed heat and the condensing heat of the ORC reduce. However, the inlet temperature of the cooling water and its mass flow rate remain unchanged, so that more gas is condensed, leading to a lower pressure. Since the

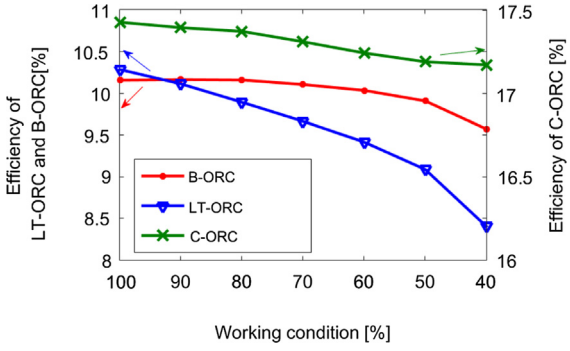

Fig. 17. The efficiencies of the three single-stage ORCs under seven typical engine working conditions.

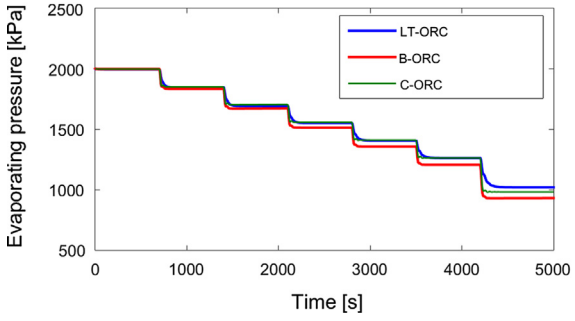

Fig. 18. The variation of evaporating pressures of the three single-stage ORCs under seven typical engine working conditions.

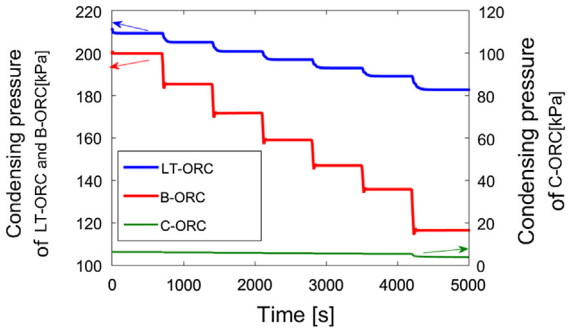

Fig. 19. The variation of condensing pressures of the three single-stage ORCs under seven typical engine working conditions.

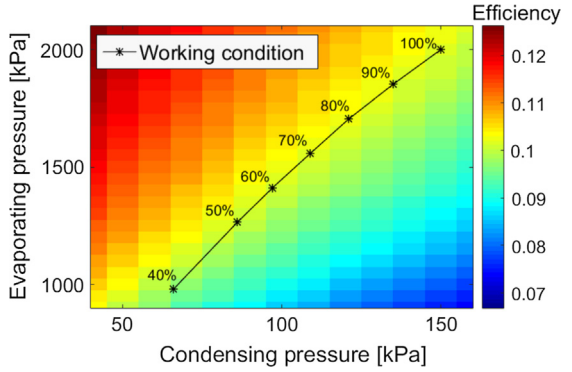

Fig. 20. The variation of the efficiency of toluene with condensing pressure and evaporating pressure.

condensing temperature declines with the decreasing condensing pressure, the heat transfer temperature difference between cold and hot fluids shrinks with the reduction of heat transfer ability. Then another balance is researched in the condenser. The condensing temperature of the LT-ORC and the C-ORC (308 K) is close to the cooling water inlet temperature (298 K), so the average temperature difference between them is quite small. This means that a small change in condensing temperature can have a great effect on the average heat transfer temperature difference, which obviously affects condensing performance. As a result, the condensing temperature or pressure only needs to change by a small amount to balance the cooling load when the engine work condition varies. By contrast, there is a large heat transfer temperature difference between the working fluid (409.5 K condensing temperature) and cooling water (358 K) in the B-ORC. Therefore, when the cooling load changes, the condensing temperature must change by a much larger amount to reach the new balance. Accordingly, the condensing pressure also has a greater variation. It is well known that lowering the condensing pressure contributes to improving output

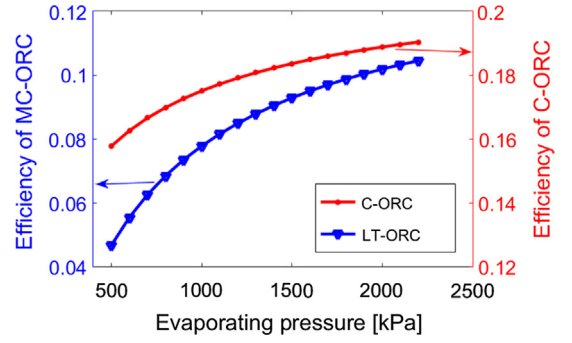

Fig. 21. The efficiencies of toluene and R245fa under different evaporating pressures.

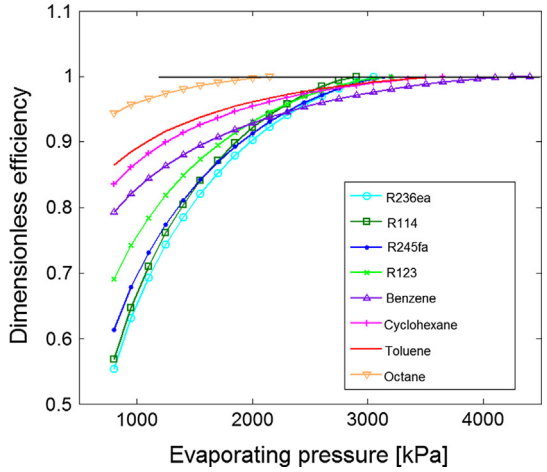

Fig. 22. The dimensionless efficiencies of different working fluids varying with evaporating pressure.

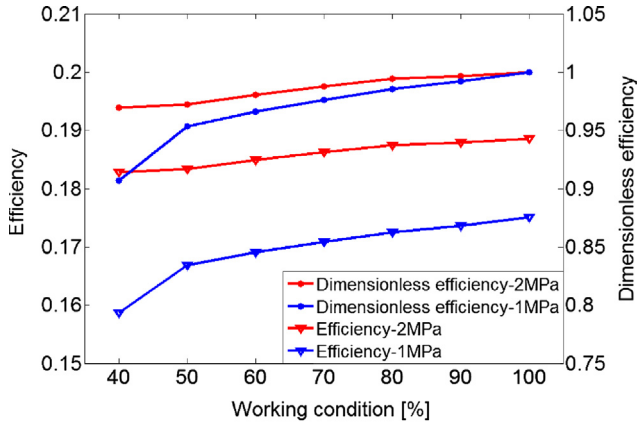

Fig. 23. The variation of system efficiency with engine working conditions under different design evaporating pressures.

power. As a result, although the B-ORC evaporating pressure decreases fastest with the dropping engine working condition, the declining condensing pressure makes the system efficiency only reduce a little, as shown in Fig. 17, and even produces a small increase under the 90% working condition. Fig. 20 shows the thermal efficiency of toluene under different evaporating pressures and condensing pressures. The states of the B-ORC under the seven engine working conditions are marked to show the thermal efficiency variation.

The decrease of the C-ORC efficiency is only slightly greater than that of the B-ORC. Fig. 21 describes the thermal efficiency of R245fa and toluene varying with evaporating pressure. It can be seen that in the range of 1–2 MPa, the efficiency of toluene does not change obviously. Therefore, the efficiency of the C-ORC only declines slightly when the engine working condition decreases. Owing to the great decrease of condensing pressure, the B-ORC efficiency declines more slowly. For the working fluid R245fa, the efficiency changes much faster with the evaporating pressure, so the LT-ORC output power reduces the fastest. For most of the working fluids, efficiency increases with rising evaporating pressure fast at first, and then more and more slowly as shown in Fig. 22 (subcritical cycles and 308 K condensing temperature for all). The flat areas of the various working fluids lie in different ranges and some of them, like toluene and cyclohexane, exist in relative low evaporating pressure.

Based on the effects of the design evaporating pressure as analyzed above, it can be known that if the design evaporating pressure is high enough to make it in the flat area under all conditions, it will help to maintain good part-load performance. Although the high design evaporating pressure may not bring an obvious increase in output power under design conditions as shown in Fig. 22, it can improve the part-load performance. Fig. 23 compares the part-load performance of two C-ORCs designed at 1 MPa and 2 MPa evaporating pressures. Obviously, the latter has better performance.

In a word, the LT-ORC has the worst part-load performance because its efficiency decreases the fastest with the declining engine working condition. By contrast, the efficiencies of the C-ORC and the B-ORC only decrease slightly. This is especially true of the B-ORC, of which the efficiency even increases slightly under 90% working condition, owing to the great decrease of condensing pressure. However, the absorbed heat of the C-ORC is always larger than that of the B-ORC, so the output power of the C-ORC decreases slowest.

4.2. The comparison with the DORC

Despite the C-ORC having the best part-load performance and the largest output power, the pressure ratio in the turbine is so large that manufacturing the turbine is difficult. The pressure ratios in the two stages of the DORC are both much smaller than those in the C-ORC and can still output a large amount of power. As shown in Table 4, the DORC output power under the rated working conditions is slightly greater than even that of the C-ORC. In this part, the DORC part-load performance is compared with the former three systems in detail. The DORC is a combination of the B-ORC and LT-ORC, so the design evaporating pressures and condensing pressures of the HT and LT stages are kept identical to those of the B-ORC (2000 kPa/200 kPa) and LT-ORC (2000 kPa/211 kPa) to allow intuitive comparison.

Table 4 describes the dimensionless output power and thermal efficiency of the four systems under seven typical engine working conditions. The definitions of dimensionless thermal efficiency and dimensionless output power are the same. From the table, it can be seen that the dimensionless thermal efficiency of the DORC is quite similar to the B-ORC, but slightly smaller. The mass flow rate and the inlet temperature of the cooling water remain unchanged all the time in the B-ORC, while the condensing heat of the HT stage is taken away by the LT stage. When the engine working condition declines, both the mass flow rate of the LT working fluid and its evaporating pressure decrease, resulting in the temperature decrease of the HT cooling water. The temperature drop can intensify the decrease of the HT stage condensing

Table 4
The comparison of DORC part-load performance with the other three systems.

Working condition	100%	90%	80%	70%	60%	50%	40%
Dimensionless power LT-ORC	1 (71.6 kW)	0.897	0.791	0.697	0.604	0.512	0.366
Dimensionless power DORC	1 (133.8 kW)	0.908	0.820	0.732	0.646	0.565	0.417
Dimensionless power B-ORC	1 (70.7 kW)	0.901	0.819	0.723	0.640	0.552	0.398
Dimensionless power C-ORC	1 (131.3 kW)	0.911	0.822	0.736	0.650	0.568	0.437
Dimensionless efficiency LT-ORC	1 (10.28%)	0.983	0.962	0.940	0.915	0.883	0.817
Dimensionless efficiency DORC	1 (19.24%)	0.999	0.995	0.992	0.983	0.974	0.953
Dimensionless efficiency B-ORC	1 (10.16%)	1.01	1.01	0.994	0.987	0.975	0.942
Dimensionless efficiency C-ORC	1 (18.86%)	0.997	0.994	0.987	0.983	0.974	0.972

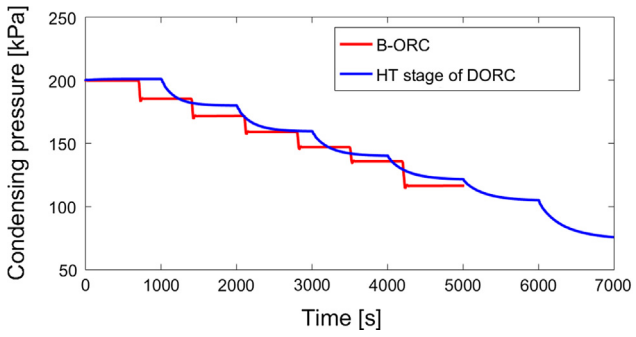

Fig. 24. The comparison between the condensing pressures of B-ORC and HT stage in DORC.

pressure. From Fig. 24, it can be found that the condensing pressure of the HT stage clearly declines faster than that of the B-ORC. This makes the HT-stage efficiency higher than that of the B-ORC. It should be noted that since the dynamic response speed of the DORC is slow [36], the engine working condition decreases every 1000 s in Fig. 24. At the same time, the efficiency of the LT stage decreases the fastest as mentioned above. Due to these two factors, the DORC efficiency is quite close to the B-ORC efficiency under different working conditions.

Comparing the dimensionless output power, it can be found that although the dimensionless efficiency of the DORC is slightly less than that of the B-ORC under part-load, its dimensionless power is slightly larger and quite close to that of the C-ORC. This indicates that the absorbed heat of the DORC is slightly greater than that of the B-ORC. As shown in Fig. 24, the condensing pressure of the HT stage decreases faster than that of the B-ORC, so the HT working fluid temperature at the evaporator inlet decreases faster as well, which contributes to enlarging the heat transfer temperature difference in the evaporator and improving the heat transfer ability. As a result, the absorbed heat of the DORC is larger under part-load.

In short, the DORC has not only the largest output power under the design working condition, but also excellent part-load performance. From the T-s diagram (Fig. 4), it can be seen that the DORC and C-ORC match with the exhaust heat better than the other two systems, and also have better performance under design and part-load working conditions. Therefore, it is believed that the system that best matches with the heat source not only performs well under the design conditions, but also has excellent part-load performance.

5. Conclusion

The part-load performance of four different forms of ORCs is compared in the study using dynamic math models. The four forms of ORC are the ORC applying low temperature working fluid R245fa with a medium heat transfer cycle (LT-ORC), the ORC applying high temperature working fluid toluene with high condensing pressure (B-ORC) and low condensing pressure (C-ORC), and the double-stage ORC (DORC). It is regarded that the more slowly the output power decreases, the better part-load performance it has. Based on the analysis above, it can be concluded that:

1 The part-load performance of the four systems decreases in the order: C-ORC > DORC > B-ORC > LT-ORC. Among the three single stage ORCs, the efficiency of the LT-ORC decreases obviously with the declining engine working condition, leading to the worst part-load performance. By contrast, the efficiencies of the C-ORC and the B-ORC only decrease a little, especially the B-ORC of which the efficiency even slightly increases under the 90% working condition. However, the absorbed heat of the C-ORC is larger than that of the B-ORC all the time, so the C-ORC has the best part-load performance. The DORC is a cascade utilization system and its part-load performance is almost as good as that of the C-ORC.
2 The condensing condition has a great impact on part-load performance. The large temperature difference between the cooling water and the condensing temperature can lead to a great drop of the condensing pressure when the engine working condition decreases, which contributes to improving the ORC efficiency under part-load. Owing to this, the efficiency of the B-ORC only declines a little and even has a slight increase under the 90% working condition.
3 The design evaporating pressures of different working fluids also greatly affect part-load performance. The efficiencies of most working fluids have a flat area where the efficiency varies slightly with evaporating pressure. The area exists in a different evaporating pressure range for various working fluids. If the design evaporating pressure is sufficiently high, it will make the evaporating pressure under all working conditions in the flat area, which helps to maintain excellent part-load performance. Although the high design evaporating pressure may not bring an obvious increase of output power under the design condition, it can improve part-load performance.
4 According to the T-s diagram, the DORC and C-ORC show the best part-load performance and have a better matching structure with exhaust. Therefore, it is believed that the system that best matches with the heat source not only performs well under the design conditions, but also has excellent part-load performance.

Acknowledgements

This work was supported by the State Key Program of National Natural Science Foundation of China (No. 51636005).

References

[1] Ibarra M, Rovira A, Alarcón-Padilla DC, Blanco J. Performance of a 5 kWe Organic Rankine Cycle at part-load operation. Appl Energy 2014;120:147–58.
[2] Uusitalo A, Honkatukia J, Turunen-Saaresti T, Larjola J. A thermodynamic analysis of waste heat recovery from reciprocating engine power plants by means of Organic Rankine Cycles. Appl Therm Eng 2014;70(1):33–41.
[3] Gewald D, Siokos K, Karellas S, Spliethoff H. Waste heat recovery from a landfill gas-fired power plant. Renew Sustain Energy Rev 2012;16(4):1779–89.
[4] Yu G, Shu G, Tian H, Huo Y, Zhu W. Experimental investigations on a cascaded steam-/organic-Rankine-cycle (RC/ORC) system for waste heat recovery (WHR) from diesel engine. Energy Convers Manage 2016;129:43–51.
[5] Sprouse III C, Depcik C. Review of organic Rankine cycles for internal combustion engine exhaust waste heat recovery. Appl Therm Eng 2013;51(1–2):711–22.
[6] Algieri A, Morrone P. Comparative energetic analysis of high-temperature subcritical and transcritical Organic Rankine Cycle (ORC). A biomass application in the Sibari district. Appl Therm Eng 2012;36:236–44.
[7] Turboden, Turboden ORC plants for Industrial Heat Recovery. < http://www.turboden.eu/en/public/downloads/12-COM.P-21-rev.23.pdf > ; 2015.
[8] Shu G, Wang X, Tian H. Theoretical analysis and comparison of rankine cycle and different organic rankine cycles as waste heat recovery system for a large gaseous fuel internal combustion engine. Appl Therm Eng 2016;108:525–37.
[9] Invernizzi Costante Mario, Sheikh Nadeem Ahmed. High-efficiency small-scale combined heat and power organic binary Rankine cycles. Energies 2018;11(4):994.
[10] Vaja I, Gambarotta A. Internal combustion engine (ICE) bottoming with organic Rankine cycles (ORCs). Energy 2010;35(2):1084–93.
[11] Shu G, Yu G, Tian H, Wei H, Liang X. A multi-approach evaluation system (MA-ES) of Organic Rankine Cycles (ORC) used in waste heat utilization. Appl Energy 2014;132:325–38.
[12] Wang T, Zhang Y, Peng Z, Shu G. A review of researches on thermal exhaust heat recovery with Rankine cycle. Renew Sustain Energy Rev 2011;15(6):2862–71.
[13] El Chammas R, Clodic D. Combined cycle for hybrid vehicles (No. 2005-01-1171). SAE technical paper; 2005.
[14] Fu BR, Hsu SW, Lee YR, Hsieh JC, Chang CM, Liu CH. Effect of off-design heat source temperature on heat transfer characteristics and system performance of a 250-kW organic Rankine cycle system. Appl Therm Eng 2014;70(1):7–12.
[15] Badescu V, Aboaltabooq MHK, Pop H, Apostol V, Prisecaru M, Prisecaru T. Design and operational procedures for ORC-based systems coupled with internal combustion engines driving electrical generators at full and partial load. Energy Convers Manage 2017;139:206–21.
[16] Bamgbopa MO, Uzgoren E. Numerical analysis of an organic Rankine cycle under steady and variable heat input. Appl Energy 2013;107:219–28.
[17] Danov SN, Gupta AK. Modeling the performance characteristics of diesel engine based combined-cycle power plants—part I: mathematical model. J Eng Gas Turb

Power 2004;126(1):28–34.
[18] Horst TA, Tegethoff W, Eilts P, Koehler J. Prediction of dynamic Rankine Cycle waste heat recovery performance and fuel saving potential in passenger car applications considering interactions with vehicles' energy management. Energy Convers Manage 2014;78:438–51.
[19] Mazzi N, Rech S, Lazzaretto A. Off-design dynamic model of a real Organic Rankine Cycle system fuelled by exhaust gases from industrial processes. Energy 2015;90:537–51.
[20] Larsen U, Pierobon L, Haglind F, Gabrielii C. Design and optimization of organic Rankine cycles for waste heat recovery in marine applications using the principles of natural selection. Energy 2013;55:803–12.
[21] Mikielewicz D, Mikielewicz J. A thermodynamic criterion for selection of working fluid for subcritical and supercritical domestic micro CHP. Appl Therm Eng 2010;30(16):2357–62.
[22] Roedder M, Neef M, Laux C, Priebe KP. Systematic fluid selection for organic rankine cycles and performance analysis for a combined high and low temperature cycle. J Eng Gas Turb Power 2016;138(3):031701.
[23] Shu G, Li X, Tian H, Liang X, Wei H, Wang X. Alkanes as working fluids for high-temperature exhaust heat recovery of diesel engine using organic Rankine cycle. Appl Energy 2014;119:204–17.
[24] Tchanche BF, Lambrinos G, Frangoudakis A, Papadakis G. Low-grade heat conversion into power using organic Rankine cycles–a review of various applications. Renew Sustain Energy Rev 2011;15(8):3963–79.
[25] Vaja I. Definition of an object oriented library for the dynamic simulation of advanced energy systems: methodologies, tools and application to combined ICE-ORC power plants (Doctoral dissertation, Università di Parma, Dipartimento di Ingegneria Industriale); 2009.
[26] Drescher U, Brüggemann D. Fluid selection for the Organic Rankine Cycle (ORC) in biomass power and heat plants. Appl Therm Eng 2007;27(1):223–8.
[27] Michos CN, Lion S, Vlaskos I, Taccani R. Analysis of the backpressure effect of an Organic Rankine Cycle (ORC) evaporator on the exhaust line of a turbocharged heavy duty diesel power generator for marine applications. Energy Convers Manage 2017;132:347–60.
[28] Lai NA, Wendland M, Fischer J. Working fluids for high-temperature organic Rankine cycles. Energy 2011;36(1):199–211.
[29] Siddiqi MA, Atakan B. Alkanes as fluids in Rankine cycles in comparison to water, benzene and toluene. Energy 2012;45(1):256–63.
[30] Invernizzi C, Iora P, Silva P. Bottoming micro-Rankine cycles for micro-gas turbines. Appl Therm Eng 2007;27(1):100–10.
[31] Invernizzi C, Iora P, Manzolini G, Lasala S. Thermal stability of n-pentane, cyclopentane and toluene as working fluids in organic Rankine engines. Appl Therm Eng 2017;121:172–9.
[32] Chinese D, Meneghetti A, Nardin G. Diffused introduction of Organic Rankine Cycle for biomass-based power generation in an industrial district: a systems analysis. Int J Energy Res 2004;28(11):1003–21.
[33] Rentizelas A, Karellas S, Kakaras E, Tatsiopoulos I. Comparative techno-economic analysis of ORC and gasification for bioenergy applications. Energy Convers Manage 2009;50(3):674–81.
[34] Liang Y, Shu G, Tian H, Wei H, Liang X, Liu L, et al. Theoretical analysis of a novel electricity–cooling cogeneration system (ECCS) based on cascade use of waste heat of marine engine. Energy Convers Manage 2014;85:888–94.
[35] Shu G, Wang X, Tian H, Liang Y, Liu Y, Liu P. Analysis of an electricity-cooling cogeneration system for waste heat recovery of gaseous fuel engines. Sci China Technol Sci 2015;58(1):37–46.
[36] Wang X, Shu G, Tian H, Liu P, Jing D, Li X. Dynamic analysis of the dual-loop Organic Rankine Cycle for waste heat recovery of a natural gas engine. Energy Convers Manage 2017;148:724–36.
[37] Luong D, Tsao TC. Linear quadratic integral control of an organic rankine cycle for waste heat recovery in heavy-duty diesel powertrain. In: IEEE American Control Conference (ACC); 2014. p. 3147–52.
[38] Jensen JM, Tummescheit H. Moving boundary models for dynamic simulations of two-phase flows. In: Proceedings of the 2nd international modelica conference, Otter, M; 2002. p. 235–44.
[39] Wei D, Lu X, Lu Z, Gu J. Dynamic modeling and simulation of an Organic Rankine Cycle (ORC) system for waste heat recovery. Appl Therm Eng 2008;28(10):1216–24.
[40]] Peralez J, Tona P, Sciarretta A, Dufour P, Nadri M. Towards model-based control of a steam rankine process for engine waste heat recovery. In: Vehicle power and propulsion conference (VPPC), IEEE, 2012 IEEE; 2012. p. 289–94.
[41] Zhiqi Wang. Experimental study and dynamic performance simulation for low-temperature waste heat generation system based on organic rankine cycle. PhD thesis in Industrial Engineering, Central South University, China; 2012 [in Chinese].
[42] Briggs DE, Young EH. Convection heat transfer and pressure drop of air flowing across triangular pitch banks of finned tubes. Chem Eng Prog Symp Ser 1963;59(41):1–10.
[43] Shiming Yang. Heat transfer, Beijing, higher education pressure; 1998. p. 162–75 [in Chinese].
[44] VDI-Gesellschaft Verfahrenstechnik und Chemieingenieurwesen. VDI Wärmeatlas, 8th ed. Berlin Heidelberg New York: Springer; 1997 [German].
[45] Peralez J, Tona P, Lepreux O, Sciarretta A, Voise L, Dufour P, et al. Improving the control performance of an organic rankine cycle system for waste heat recovery from a heavy-duty diesel engine using a model-based approach. In: Decision and Control (CDC), 2013 IEEE 52nd Annual Conference on IEEE; 2013. p. 6830–6.
[46] Ahlgren F, Mondejar ME, Genrup M, Thern M.. Waste heat recovery in a cruise vessel in the Baltic Sea by using an organic Rankine cycle: a case study. In: ASME Turbo Expo 2015: Turbine Technical Conference and Exposition, American Society of Mechanical Engineers; 2015. p. V003T06A018-V003T06A018.
[47] Manente G, Toffolo A, Lazzaretto A, Paci M. An Organic Rankine Cycle off-design model for the search of the optimal control strategy. Energy 2013;58:97–106.
[48] Horst TA, Rottengruber HS, Seifert M, Ringler J. Dynamic heat exchanger model for performance prediction and control system design of automotive waste heat recovery systems. Appl Energy 2013;105:293–303.
[49] Li YR, Wang JN, Du MT. Influence of coupled pinch point temperature difference and evaporation temperature on performance of organic Rankine cycle. Energy 2012;42(1):503–9.
[50] Wang X, Shu G, Tian H, Liu P, Jing D, Li X. The effects of design parameters on the dynamic behavior of organic ranking cycle for the engine waste heat recovery. Energy 2018;147:440–50.